Emadi, F.; Vuorinen, V.; Mertin, S.; Widell, Kim; Paulasto-Kröckel, M.

Microstructural and mechanical characterization of Cu/Sn SLID bonding utilizing Co as contact metallization layer

Published in:
Journal of Alloys and Compounds

DOI:
10.1016/j.jallcom.2022.167228

Published: 25/12/2022

Document Version
Publisher's PDF, also known as Version of record

Journal of Alloys and Compounds 929 (2022) 167228

Contents lists available at ScienceDirect

Journal of Alloys and Compounds

journal homepage: www.elsevier.com/locate/jalcom

Research Article

Microstructural and mechanical characterization of Cu/Sn SLID bonding utilizing Co as contact metallization layer

F. Emadi[a,*], V. Vuorinen[a], S. Mertin[b], K. Widell[c], M. Paulasto-Kröckel[a]

[a] Department of Electrical Engineering and Automation, School of Electrical Engineering, Aalto University, PO Box 13340, FI-00076 Aalto, Finland
[b] VTT Technical Research Centre of Finland, P.O. Box 1000, VTT, FI-02044 Espoo, Finland
[c] Department of Mechanical Engineering, School of Engineering, Aalto University, P.O. Box 11000, FI-00076 Aalto, Finland

ARTICLE INFO

Article history:
Received 27 June 2022
Received in revised form 24 August 2022
Accepted 14 September 2022
Available online 16 September 2022

Keywords:
Wafer-level bonding
3D integration
Cu-Sn SLID bonding
TLP bonding
Microstructural evolution
Cu-Co-Sn system

ABSTRACT

Most micro-electro-mechanical systems (MEMS) devices contain fragile moving parts, which poses challenges in process integration of interconnection methods requiring wet-chemistry, such as solid-liquid interdiffusion bonding (SLID). These sensitive MEMS structures can be protected from either the wet-chemistry or plated metals during chemical/electro-chemical plating of SLID interconnection materials; however, this is a complex process. Hence, our previous research has investigated employing a physically deposited contact metallization on the wafers containing functional devices instead of chemically deposited layers (such as electrochemical Cu). Co is a plausible contact metallization layer for Cu-Sn SLID bonding, as it is chemically compatible with Cu–Sn systems. Furthermore, it can positively impact the mechanical reliability of the intermetallic compounds (IMCs) due to the stabilizing of the HT-hexagonal Cu_6Sn_5 phase down to room temperature and suppressing the Cu_3Sn phase formation and subsequent void formation. However, it is critical to control Co thickness to achieve a stable bond based on our previous research on Co bulk in contact with Cu-Sn electroplated silicon chips. To utilize Co as a contact metallization layer for wafer-level Cu-Sn SLID bonding, it is necessary to define appropriate metal layers in the contact metallization stack. Consequently, the present study investigated four different contact metallization stacks including A) 40nmTi/100 nm Co, B) 40 nm Ti/200 nm Mo/100 nm Co, C) 40 nm Ti/500 nm Co, and D) 40 nm Ti/200 nm Mo/500 nm Co. More specifically, we evaluated the microstructural formation and evolution and mechanical performance of the joints. Our study revealed that the Ti/Mo/100 nm Co contact metallization stack for (4 µm)Cu/(2 µm)Sn SLID bonding is composed of IMCs $(Cu,2.5at\%Co)_6Sn_5$ and Cu_3Sn without remaining Sn. Moreover, the joint contained a negligible number of voids even after long-time annealing at 150 °C. Our analysis of the mechanical properties of the joint showed that 1) the tensile fracture surface exhibited a mixture of ductile and brittle fractures, and 2) the Young's modulus of $(Cu,2.5at\%Co)_6Sn_5$ was higher than Cu_6Sn_5, while hardness of $(Cu,2.5at\%Co)_6Sn_5$ and Cu_6Sn_5 were comparable. By employing a Ti/Mo/100 nm Co contact metallization stack, the current study was able to produce 25 µm and 10 µm void free (4 µm Cu/2 µm Sn) microbumps.

1. Introduction

The structural elements and the unique operational environment of most microelectromechanical systems (MEMS) have introduced significant challenges to the packaging. Many MEMS devices require a hermetic packaging with preferably no postprocessing after the MEMS device is released [1–3]. In addition, for some MEMS devices (e.g., CMOS-MEMS devices), it is crucial to limit the heat load on the wafers [4]. In this regard, solid-liquid interdiffusion (SLID) bonding is an attractive process for MEMS packaging due to its high hermeticity, low bonding temperature, and high re-melting temperature [4,5]. However, as most MEMS devices contain fragile parts and operate in harsh environments – which bring wider variety of failure mechanisms compared to traditional semiconductor microelectronics – the reliability of SLID bonding and complete interconnection materials require evaluation. The reliability performance of SLID bonding significantly depends on the bond quality and mechanical properties of the IMCs formed at the joint area, as different type of defects, such as cracks and voids, can seriously degrade the mechanical properties of the brittle IMCs. Therefore, it is of utmost

Abbreviations: SLID, solid liquid interdiffusion; IMC, intermetallic compound; MEMS, microelectromechanical systems; FE-SEM, field emission scanning electron microscope; FE-SEM, energy-dispersive X-ray spectroscopy

* Corresponding author.
E-mail address: fahimeh.emadi@aalto.fi (F. Emadi).

https://doi.org/10.1016/j.jallcom.2022.167228

importance to clarify the bond quality and microstructural evolution and mechanical properties of the intermetallic compounds formed in the bonding area [5–7].

Cu-Sn SLID bonding is one of the most widely studied SLID systems, as it is mature and low cost [5,6]. Cu_3Sn and Cu_6Sn_5 formation (with re-melting points of 676 °C and 450 °C, respectively) in Cu-Sn systems has been reported in various studies. The first intermetallic forms in Cu-Sn SLID bonding is Cu_6Sn_5, followed by the nucleation of Cu_3Sn at the Cu/Cu_6Sn_5 interface [8–10]. However, it has been shown that the formation of the Cu_3Sn IMC in the Cu-Sn joints is accompanied by voids evolution at the Cu/Cu_3Sn interface and inside the Cu_3Sn IMC, which can degrade the bond strength and hermiticity [11–14]. The common reasons for void formation during annealing are trace impurities in the electroplating solutions and Kirkendall voids due to the imbalance in the interdiffusion of Cu and Sn inside the IMCs [15–18]. Many studies have been conducted to investigate how to inhibit void formation. These studies have suggested that controlling the electroplating parameters, such as additives and the age of electroplating solution, and adding sulfide-forming elements in the solder can limit void formation to a negligible amount [18–21]. Herein, we provide a few examples of the recent progresses in the void suppression of Cu-Sn (or Sn based solder) systems as follows. G. Ross et al. reported that utilizing a high-pure electrolyte with medium current density during the electroplating process minimizes the void formation in the Cu-Sn electroplated system [17], [18]. P. C. Chiang et al. investigated the effect of Cu orientation in Cu film with twin boundaries on the void suppression in SAC305/Cu system during thermal aging: Σ3 twin boundary in the bamboo structure with ⟨111⟩-preferred orientation showed greater suppressing effect on the Kirkendall voids than that in ⟨110⟩-preferred Cu films [22].

Furthermore, it has been shown that introducing a third element, such as Ni, Au, In and Zn, to the Cu-Sn system suppresses Cu_3Sn formation and the following evolution of voids [23–25]. For instance, S. U. Mehreen et al. investigated the effect of various alloying elements (Ni, Zn, Au, Sb and In) on the Suppression of the Cu_3Sn Phase in Sn-10 wt%Cu Alloys [26]. Based on their studies, all these alloying elements, except Sb, suppressed the Cu_3Sn IMC formation. However, Ni and Zn showed the significant suppression effect on the Cu_3Sn formation [26]. Hence, as far as the void formation in the joints is concerned, $Cu/Cu_6Sn_5/Cu$ and $Cu/Cu_3Sn/Cu_6Sn_5/Cu_3Sn/Cu$ is preferred to $Cu/Cu_3Sn/Cu$. However, there are still other possible reliability issues of Cu-Sn SLID bonding containing Cu_6Sn_5 IMC. For example, internal stresses can be generated by the volumetric change due to the transformation of HT-hexagonal Cu_6Sn_5 to LT-monoclinic Cu_6Sn_5 during aging [27,28]. Nonetheless, this phenomenon can be controlled by stabilizing the HT-hexagonal phase down to room temperature via introducing a third element (such as Ni, Au, In, and Zn) to the Cu-Sn SLID bonding system [16,25,27,29]. For instance, A. Rautiainen et al. reported the drastic impact of Pt on the stabilization of HT-hexagonal Cu_6Sn_5 phase [30]. Nonetheless, in addition to the microstructural evolution and the bond quality, understanding the mechanical behavior of the Cu-Sn SLID system is of utmost importance to design a mechanical reliable bond.

Intensive research has been conducted to study the mechanical properties and strength of the Cu-Sn IMCs [31–33]. According to J. Feng et al. [33], the average values of hardness (H) and Young's modulus (E) of Cu_6Sn_5 and Cu_3Sn are (120.337 ± 3.789 and 5.608 ± 0.313 GPa) and (139.907 ± 3.693 and 5.321 ± 0.675 GPa), respectively. According to Milman et al., the fraction of plastic deformation in the total deformation during indentation (δ_H) can be used as a plasticity characteristic of brittle materials [34]. δ_H can be determined by the ratio of Young's modulus to hardness (high E/H value implies better plasticity for IMCs, while low E/H indicates brittleness) [7], [34–36]. Hence, Cu_3Sn shows better plasticity compared to Cu_6Sn_5, as it possesses similar hardness to and a higher Young's modulus than Cu_6Sn_5. Therefore, Cu_3Sn benefits joints from a reliability point of view if it shows high bond quality. Nevertheless, the processing time to achieve the $Cu/Cu_3Sn/Cu$ bond structure is much longer than $Cu/Cu_3Sn/Cu_6Sn_5/Cu_3Sn/Cu$, which can cause extra thermal stress and subsequently deteriorate the reliability of the packaging system. However, the development of effective approaches to shorten the bonding time has been explored in the literature [37,38]. For instance, it has been shown that obtaining a $Cu/Cu_3Sn/Cu$ joint requires a short bonding time by employing a pulsed High Frequency Electromagnetic Field (HFEF) [37]. Nonetheless, in addition to the nanoindentation analysis of the Cu-Sn SLID systems, many studies have been conducted to evaluate the mechanical properties of the Cu-Sn joints by shear/tensile strengths measurements and fractures surface examination [39–44]. It has been shown that Cu/Sn/Cu SLID joints exhibits a brittle fracture surface and a stronger strength compared to the conventional solders [39,45]. However, it has been proven that the joint shear strength significantly depends on the IMCs formed at the bondline: full Cu_3Sn IMC joint shows higher shear strength than the joint composed of Cu_6Sn_5/Cu_3Sn IMCs [43]. Nonetheless, it must be noted that even if the mechanical properties and bond quality of joints are improved, utilizing Cu-Sn SLID bonding for MEMS packaging requires some specific considerations concerning the negative impact of chemical/electro-chemical plating of the SLID bond on MEMS devices containing delicate moving parts. It is necessary to protect the sensitive MEMS structures from either the wet-chemistry or plated metals during chemical/electro-chemical plating of SLID interconnection materials, which complicates the process integration options.

As a result, utilizing Cu-Sn SLID bonding for MEMS packaging demands a physically deposited contact metallization layer/stack on the device wafers to avoid wet-process techniques (electroplating of contact metallization for Cu-Sn SLID system) [30,46]. A wide variety of chemically or physically deposited contact metallization layers (such as Cu, Ni, Ag, and Pt) have been used for Cu-Sn SLID bonding systems in the literature [30,47–50]. For instance, A. Rautiainen et al. discovered a Pt contact metallization layer for Cu-Sn SLID bonding. They reported the formation of $(Cu,Pt)_6Sn_5$, Cu_3Sn, and $PtSn_4$ IMCs in the bonding area and the stabilization of hexagonal Cu_6Sn_5 with the presence of a third element: Pt [30]. Based on their results, Pt is a potential contact metallization layer for Cu-Sn SLID bonding in MEMS packaging; however, the weak etch ability and high price of platinum bring challenges for large-scale production. In turn, when Ni is used as contact metallization layer, the main IMCs are $(xCu, (1-x)Ni)_6Sn_5$, $(xCu, (1-x)Ni)_3Sn$, and $(xNi, (1-x)Cu)_3Sn_4$, depending on the bonding condition [51–53]. As discussed, Ni suppresses Cu_3Sn formation and consequently void formation and stabilizes the hexagonal Cu_6Sn_5. Nevertheless, drawbacks in using a Ni metallization layer are namely its fast oxidization [54], stresses exerted during thick layer sputtering, and the brittleness of the IMCs.

Taking into account the specifically required considerations for some MEMS devices, such as CMOS compatibility, avoiding the chemical deposition on the device wafers, and chemical compatibility with the Cu-Sn SLID bonding, Co contact metallization is one of the plausible candidates [46]. In addition, it has been reported that Co can stabilize the HT-hexagonal Cu_6Sn_5, suppress Cu_3Sn formation, and speed up IMC formation in the Cu-Sn SLID bonding system, which can reduce the SLID processing time and cost [46,55,56]. The microstructural evolution of the Co metal in contact with Cu-Sn has been previously investigated; depending on the bonding condition, various IMCs (such as $(Cu,Co)_6Sn_5$, Cu_3Sn, (Co,Cu)Sn and $(Co,Cu)Sn_3$) can be evolved in the joint area [46,56–58]. Our previous study on the microstructural evolution of the Co bulk in contact with Cu-Sn electroplated silicon chips has shown that a fully IMC-bonded joint can be successfully achieved only if a thin layer of Co (Co thickness/ Sn thickness ≤ 4%) is in contact with the Cu-Sn SLID system. In this case, the main phases are $(Cu,Co)_6Sn_5$ and $(Cu,Co)_3Sn$.

This study also discussed crystal orientation, structure, and the relationship between formed IMCs and bonding time and temperature [46].

Previous research [46,55–57,59–61] nonetheless contains gaps regarding utilizing Co as a single contact metallization layer or part of a metallization stack for the Cu-Sn SLID bonding system. For example, amongst the available literature, the Young's modulus and hardness values of $(Cu,Co)_6Sn_5$ (which is the targeted IMC to grow in the Co-Sn-Cu system based on our previous finding s), and tensile fracture mode of the joint are lacking. Furthermore, there is no information on the microstructural evolution and the bond quality of Cu-Sn SLID bonding in contact with a thin Co layer. Therefore, the current work aims to investigate the microstructural evolution and the bond quality via the SEM-EDX of sputter deposited thin Co contact metallization as a single layer or part of a metallization stack for Cu-Sn SLID bonding utilized for MEMS devices. Furthermore, it utilizes a tensile test and nanoindentation test to study the fracture surface and the mechanical properties of the bonding, respectively.

2. Materials and methods

2.1. Specimen preparation

All samples were prepared on thermally oxidized (300 nm SiO2) 4″ Si (100) wafers. The thin-film deposition took place in a cluster sputtering system CS 730 S from Von Ardenne. A 60 nm-thick TiW adhesion layer was sputtered on cap wafers, followed by a 100 nm-thick copper seed layer sputtering. Then 4 µm of copper was electroplated utilizing NB Semi plate Cu 100 bath, followed by 2 µm of the electroplated tin using NB Semi plate Sn 100 solution from NB technologies. A 100 nm- and 500 nm-thick sputtered Co films were utilized as contact metallization on the device wafers in stacks A-B and C-D, respectively. In the device wafers stacks, A and C, a 40 nm-thick Ti adhesion layer was sputtered prior to the Co film. A 40 nm Ti/200 nm Mo metallization layers were sputtered prior to the Co contact metallization layer on the device wafers stacks B and D. The cap and device wafers were cut into 5 × 5 mm pieces (cap and device chips). Finally, the prepared chips were placed in a metal holder. They were then soldered in an air muffle furnace under 250 °C for 1 h. The samples were named as follows: Sample A (100 nm Co/Sn-Cu), Sample B (Mo-100 nm Co/Sn-Cu), Sample C (500Co/Sn-Cu), and Sample D (Mo-500 nm Co/Sn-Cu) using device wafers A, B, C, and D, respectively, for chip-level bonding. The bonding procedures regarding time and temperature were selected to mimic wafer-level bonding conditions utilized for Cu–Sn bonds. A reference sample of the Cu-Sn-Cu system was prepared by bonding two cap chips (Sample E (Cu-Sn-Cu)) in this study. In order to prepare micro-bump bonding, a cap wafer was patterned with the bump sizes of 250–10 µm, then cut into 5 × 5 mm pieces. Finally, chips were bonded to the device chips of stack B (Sample F). A schematic of the wafers and the chip-level bonded samples are shown in Fig. 1. In order to study the microstructural evolution, Sample B (Mo-100 nm Co/Sn-Cu) and Sample E (Cu-Sn-Cu) were aged at 150 °C for 1000 h. The cross-sections of all samples were prepared using standard metallographic methods.

2.2. Samples characteristics

2.2.1. Microstructural evolution

A JSM-6330 F field emission scanning electron microscope (SEM; JEOL Ltd.) with a backscattered electron (BSE) detector, an INCA X-sight energy-dispersive X-ray spectroscopy (EDX) system (Oxford Instruments), and a JIB-4700 F focused ion beam (FIB; JEOL Ltd.) with upper secondary electron (USE) imaging, were used for detailed micro-structural analysis. For cross-section analysis using SEM and EDX, samples were prepared using standard metallographic methods. The composition of phases was determined by averaging measurements from a minimum of five locations using EDX.

2.2.2. Mechanical characterization

2.2.2.1. Tensile fracture surface. A stud pull method was utilized to characterize the tensile strength of the bonds with an MTS 858 Table System that contained a Flex Test 40 Digital controller and an MTS Silent Flow HPU system. The strain rate was set on 0.1 mm/s.

2.2.2.2. Nano-indentation test. Nano-indentation test was performed within the IMCs layers at the joint area of Co/Sn/Cu and Cu/Sn/Cu stacks using a CSM Instruments Nanoindentation tester. A Berkovich diamond indenter was used with following load function parameters: 5mN maximum load, 10mN/min loading and unloading rate, and 15 s hold time. The mechanical properties of the samples were measured using the continuous data of the applied load (P) and indenter displacement (h) during the test. The Nano-

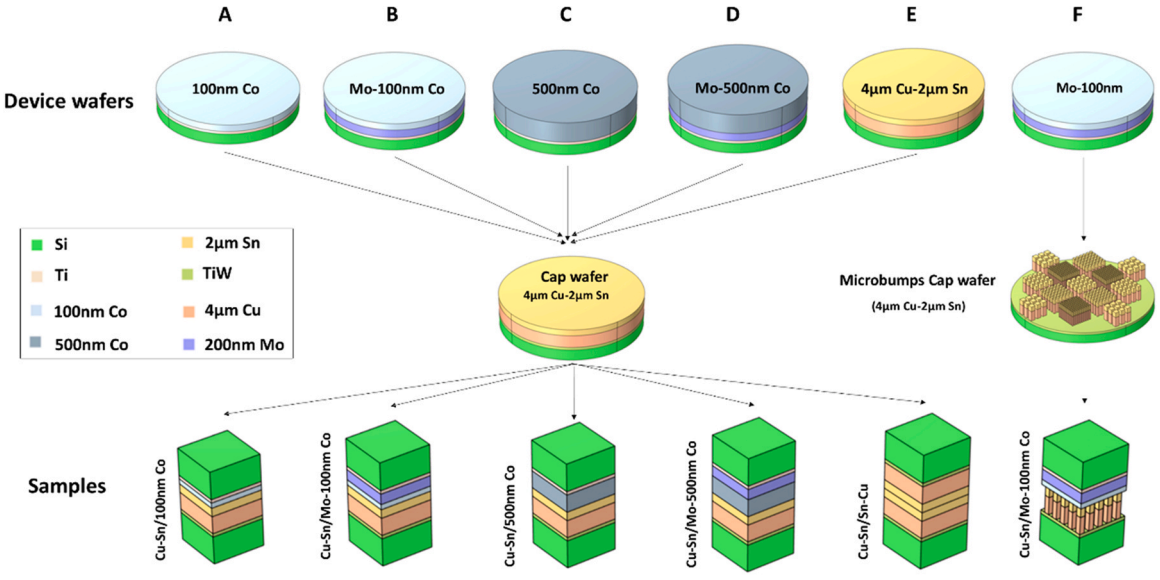

Fig. 1. A schematic illustration of the wafers and samples used in the present study.

Indentation hardness (H) and reduced elastic modulus (Er) were calculated using equations shown below:

$$H = \frac{P}{A} \quad (1)$$

$$E_r = \frac{1}{2}\frac{\sqrt{\pi}}{\sqrt{A}}\frac{dP}{dh} \quad (2)$$

Where P, A, and dP/dh signify the maximum indentation load, the projected area, and the onset slope of the unloading curve, respectively.

The young's modulus can be calculated using the following equation:

$$E_r = \left(\frac{1-\nu_s^2}{E_s} + \frac{1-\nu_i^2}{E_i}\right) \quad (3)$$

where ν_i, E_i, and ν_s are the Poisson coefficient, the elastic properties of the diamond indenter, and the Poisson coefficient of the measured phase, respectively.

3. Results and discussion

3.1. Microstructural evolution

It has been shown that the amount of Co dissolving into liquid Sn and participating in Cu-Sn IMCs formation is critical for bond quality and stability [46]. To illustrate the impact of the different contact metallization stacks with various Co thickness, Fig. 2 shows the cross-sectional BSE micrographs of Co-Sn-Cu SLID sandwiches (Sample A, B, C, and D) bonded at 250 °C for 1 h. The EDX analysis results demonstrate that the thicknesses of the metallization stack layers significantly impact the final reaction products of Cu/Sn SLID bonding and bond quality, as was predicted in our previous study (Ref [31]). The SLID bonded joint for samples A (100 nm Co/Sn-Cu) and B (Mo-100 nm Co/Sn-Cu) comprises two phases: a continuous thin layer of Cu_3Sn and a thick layer of $(Cu,Co)_6Sn_5$. Co was not detected for the Cu_3Sn IMC from the EDX analysis, and the Co content in the Cu_6Sn_5, was varied from 1 at% ± 0.5–6 at% ± 1 across the bond line. However, a large portion of the Cu_6Sn_5 formed in the bond area contained on average 2.5 at% ± 1 Co, and only Cu_6Sn_5 with 1 ± 0.5 and 6 at% ± 1 Co were identified in a couple of analyzed points. A thick layer of $(Co,Cu)Sn_3$ was identified in Sample C (500 nm Co/Sn-Cu) and D (Mo-500 nm Co/Sn-Cu). In addition, the Co content dissolved into the Cu_6Sn_5 in these samples exhibited a larger variation (9 at% ± 1 close to the device chip (Co-side) and 2.5 at% ± 1 close to the cap chip (Cu-side)). Based on the results, $(Cu,Co)_6Sn_5$ is the first IMC that appears at the Co/Sn/Cu joints interface. It has been previously reported that Co-Sn IMCs such as $CoSn_3$ are more temperature-sensitive than $(Cu,Co)_6Sn_5$. Furthermore, their growths are depressed during the initial bonding stage by Cu dissolved into the solder [46,57,59,62].

The 100nmCo/Cu-Sn stack (Sample B) was successfully bonded at 250 °C for 1 h. However, samples A (100 nm Co/Sn-Cu), C (500 nm Co/Sn-Cu), and D (Mo-500 nm Co/Sn-Cu) detached from the Ti/IMC interface, both from Ti/IMC interface and through the $(Cu,Co)_6Sn_5$, and inside the $(Cu,Co)_6Sn_5$, respectively. The reasons of the detachment from inside the $(Cu,Co)_6Sn_5$ were detailed in our previous work [35]. Furthermore, according to the results in the current study, the adhesion between Ti and IMCs is weak after the total consumption of the Co and Sn layers by IMCs formation(as seen for Sample A and

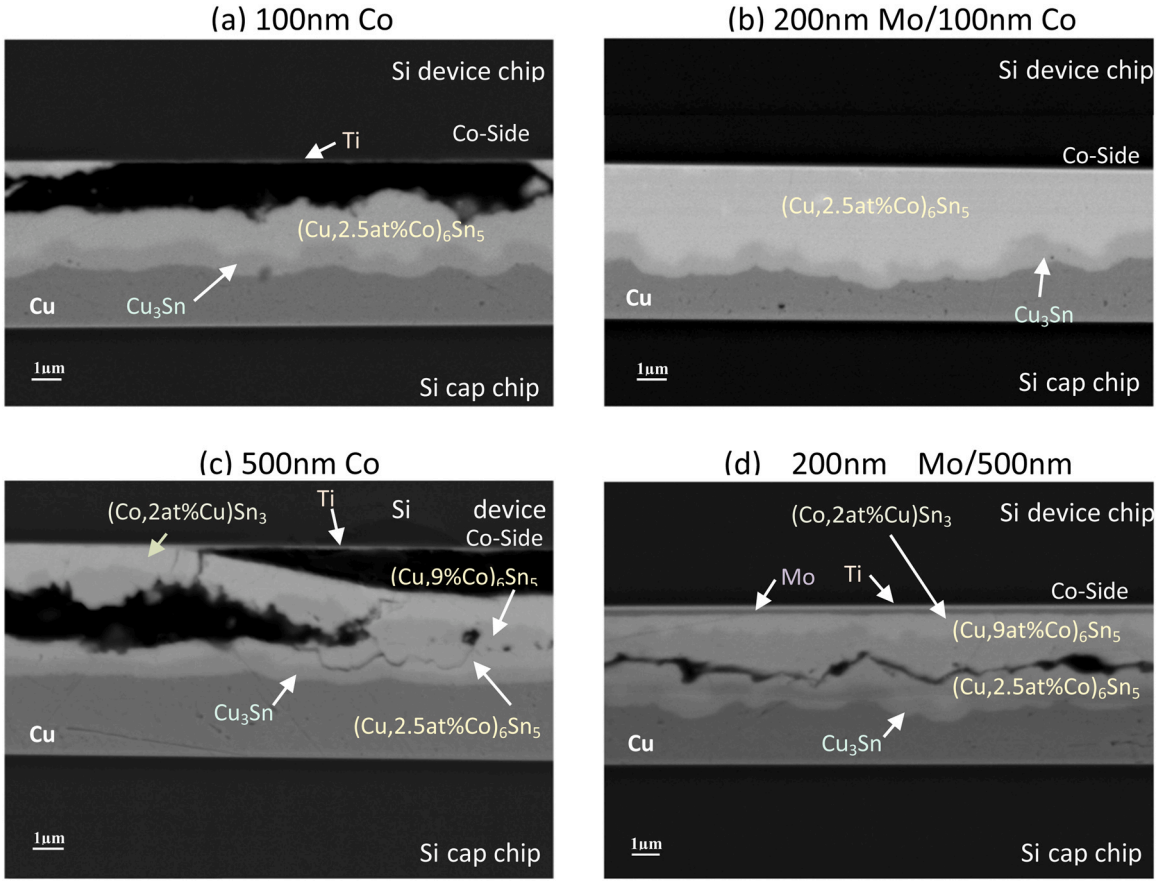

Fig. 2. Cross-sectional BSE-SEM images of Cu-Sn-Co joints formed at 250 °C for 1 h, (a) Sample A (Cu-Sn/100 nm Co), (b) Sample B (Cu-Sn/Mo-100 nm Co), (c) Sample C (Cu-Sn/500 nm Co), and (d) Sample D (Cu-Sn/Mo-500 nm Co).

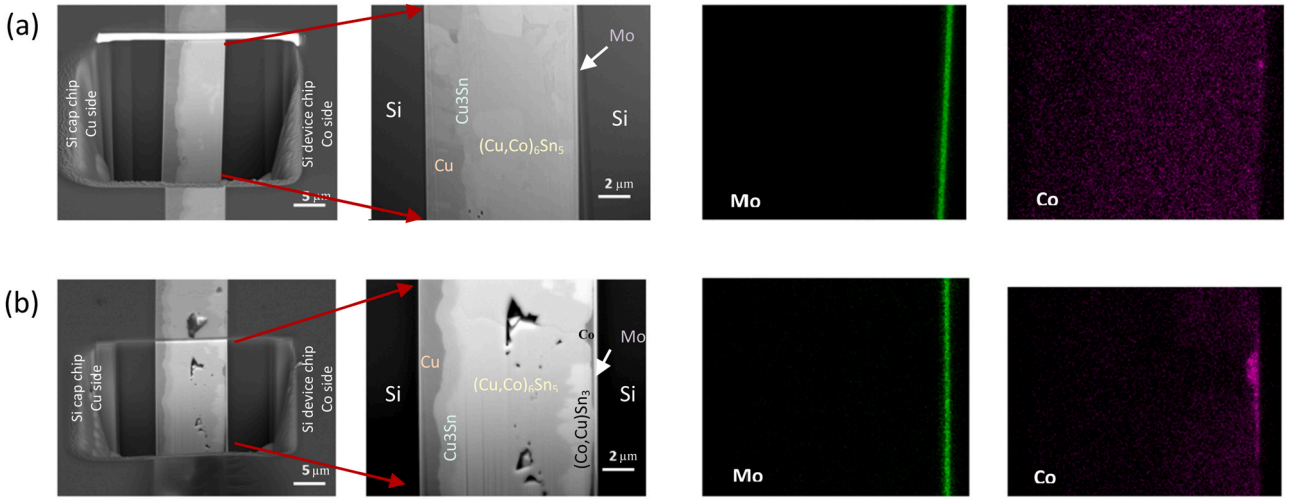

Fig. 3. USE image of a polished surface with a FIB, and EDX elemental (Mo and Co elements) mapping of (a) Sample B (Cu-Sn/Mo-100 nm Co), and (b) Sample D (Cu-Sn/Mo-500 nm Co).

Sample D). Nonetheless, the Ti/Mo layers shows strong adhesion to the IMCs.

The detachment of intermetallic compounds from interfaces between solder and the thin wetting layer used in under bump metallization (spalling phenomena) has been discussed in literature [63–69]. It has been shown that the spalling phenomena, when the large amount of solder remained, appears due to a high interfacial energy between IMCs and an adhesion layer (such as Cr and Ti) [63–66,68,69]. Furthermore, C. H. Tsai et al. showed that the spalling phenomena can be emerged even when the pure Sn has been completely consumed [67]. Based on their observation, spalling phenomena appears between the interface of the Cu-Sn intermetallics and Cr because of the high interfacial energy. It is plausible that detachment between the Ti and IMCs formed in the Cu-Sn-Co system is happened due to the high interfacial energies at the interface of Ti/IMCs. between the interface of the IMCs and Ti. While Mo/IMCs could possibly have lower interfacial energies.

Fig. 3 shows the USE images of polished surfaces with a FIB and the corresponding EDX elemental (Mo and Co) mapping of Sample B (100nmCo/Cu-Sn) and Sample D (Mo-500 nm Co/Sn-Cu). The signal of Mo in both joints was strong on top of the Ti layer; however, no signal was detected in the other areas of the joint, which indicates that Mo did not participate in the IMC formation. The cobalt corresponding elemental maps for Sample B (100nmCo/Cu-Sn) show that Co was distributed inside the Cu_6Sn_5 IMC. Nonetheless, there was no strong signal of Co at the Mo/IMCs interface, which is evidence that the Co was entirely consumed to form the IMCs in Sample B. It reveals that the thickness of the Co layer was inadequate to form Co-Sn IMCs such as $CoSn_3$, and the entire Co dissolved into Sn and formed $(Cu,Co)_6Sn_5$. However, the strong signal at the interface of the Mo/IMCs for Sample D (Mo-500 nm Co/Sn-Cu) shows that a small portion of the Co layer did not participate in the IMC formation in Sample D. Since there are a $(Cu,Co)_6Sn_5$ phase and a well-known Cu_3Sn IMC in the joint interface of successfully bonded Sample B (100nmCo/Cu-Sn), it is possible to estimate the mechanical and thermomechanical reliability of the bond by measuring the Young's modulus and hardness of the $(Cu,Co)_6Sn_5$ and Cu_3Sn and evaluating the bond quality before and after aging. As can be seen in Figs. 2-b and 3-a, the as-bonded joint shows high bond quality with no voids or cracks in the bond line.

Fig. 4 shows cross-sectional BSE micrographs and EDX elemental mapping of a polished surface with a BIB of Sample B (100nmCo/Cu-Sn) bonded at 250 °C for 1 h after aging at 150 °C for 1000 h. The strong signal Mo at the Si-joint area interface without a signal in the bonding area indicates that these element were not consumed during bonding and annealing. The Co signals illustrate the Co

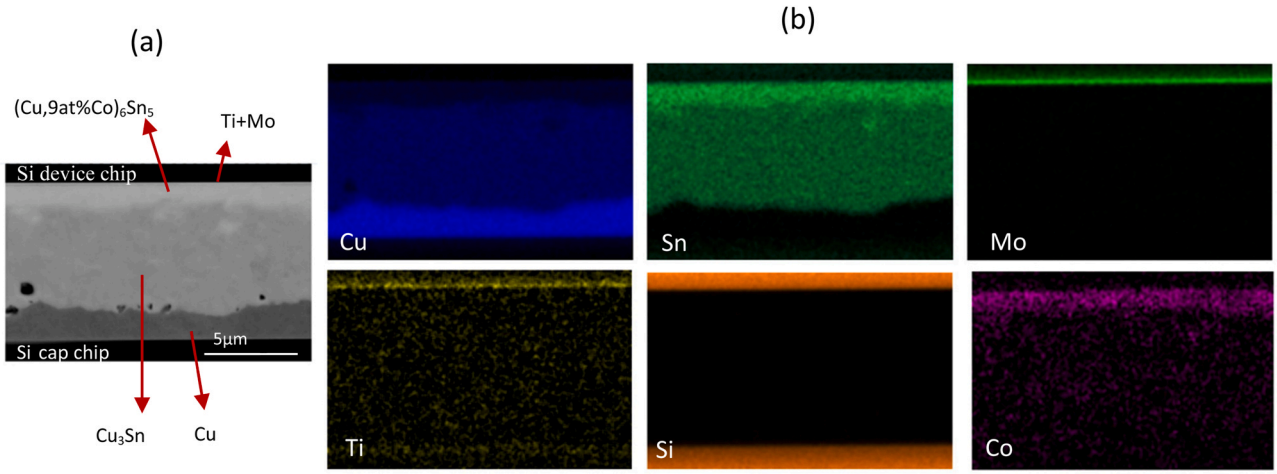

Fig. 4. (a) BSE image of a polished surface with a BIB, and EDX analysis, and (b) EDX elemental mapping of Sample B (Cu-Sn/Mo-100 nm Co) bonded at 250 °C for 1 h and annealed at 150 °C for 1000 h.

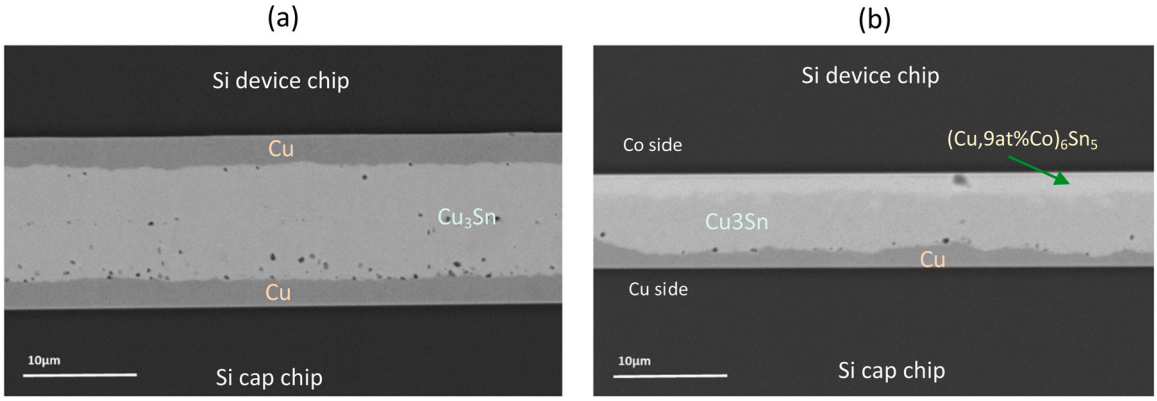

Fig. 5. BSE-SEM micrograph of (a) Sample E (Cu/Sn/Cu), and (b) Sample B (Cu-Sn/Mo-100 nm Co) after annealing at 150 °C for 1000 h.

depletion from the Cu-side of the joint and the following accumulation of the Co in the thin Cu_6Sn_5 layer in the Co-side of the bond. In turn, Fig. 5 presents the cross-sectional BSE micrographs of Cu/Sn/Cu (Sample E) and Mo-100nmCo/Cu-Sn (Sample B) joints bonded at 250 °C for 1 h after aging at 150 °C for 1000 h. The $(Cu,2.5\%Co)_6Sn_5$ phase (evolved in Sample B during bonding) mainly transformed into Cu_3Sn with Cu diffusion into the IMC layer during annealing. A thin layer of Cu_6Sn_5 with higher Co content remained close to the Co-side. The total thickness of the joint was about 8.2 μm, of which the IMCs accounted for around 6.5 μm, including 5.3 μm Cu_3Sn and 1.2 μm (Cu, 9at%Co)$_6Sn_5$. However, in pure Cu-Sn SLID system, the annealed sample was composed of single Cu_3Sn phase. Eventhogh the as-bonded Cu/Sn/Cu and Mo-100nmCo/Cu-Sn joints contained Cu_6Sn_5 and Cu_3Sn with the same fraction valumes, after annealing the Cu_3Sn valume fraction was less in the Mo-100nmCo/Cu-Sn joint (81%) than Cu/Sn/Cu (100%). The results are in a good agreement with the previously reported data: impact of Co on the stabilization of the Cu_6Sn_5 and reduction of the Cu_3Sn formation [46,70,71]. Moreover, it has be shown that the volume shrinkage by transforming Cu_6Sn_5 to Cu_3Sn is 4.38% which can induce stresses to the system [41]. Therefore, the total shrinkage that Cu-Sn SLID system normally experiences can be reduced by utilizing Co metallization layer.

It is noteworthy that only limited voiding was observed at the Cu/Cu_3Sn interface with no detectable voids either at the Co-$(Cu,Co)_6Sn_5$ interface or inside the IMCs (Figs. 4-a and 5-b). However, there were a much larger number of voids at the Cu/Cu_3Sn interface and inside the Cu_3Sn of the annealed Cu/Sn/Cu joint (Fig. 5-a). Hence, it can be concluded that Co significantly reduces void formation during annealing, which can be because of the effect of Co on the interdiffusion of Cu and Sn or the formation of the Cobalt Sulfide.

Fig. 6 shows the cross-sectional BSE-SEM images of the 10 μm and 25 μm bump (Mo-100nmCo/Sn-Cu) bonded at 250 °C for 1 h (Sample F). As can be seen in Fig. 6, a uniform void-free fully IMC (single-phase $(Cu,Co)_3Sn$) formed at the joint area. Void formation as a consequence of Cu_3Sn has been widely reported [18,21,72–74].

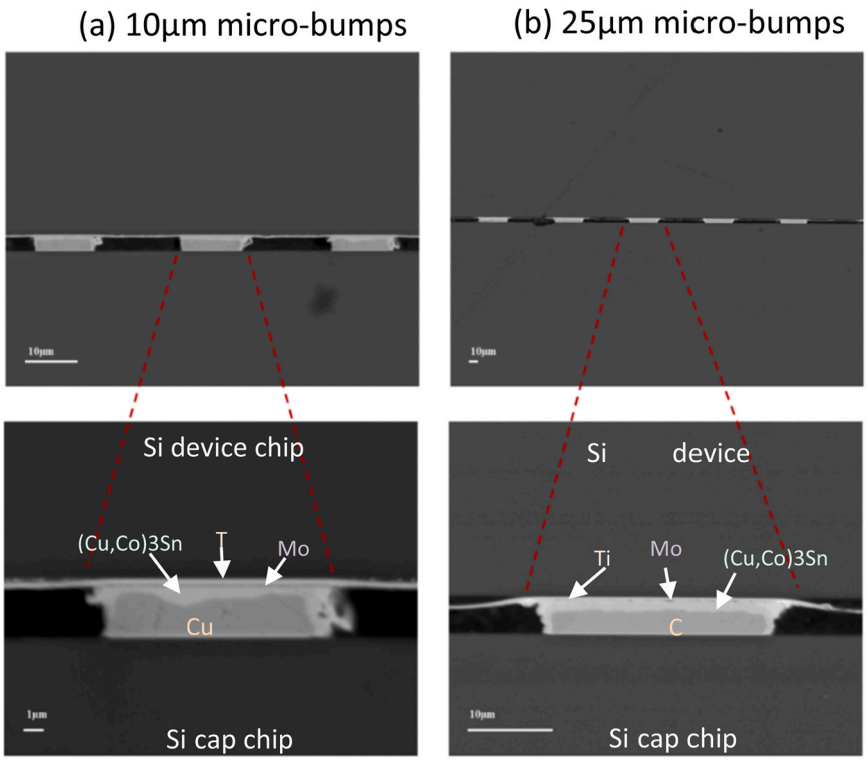

Fig. 6. Cross-sectional BSE SEM images of Cu-Sn-Co (a) 10 μm micro-bumps, (b) 25 μm micro-bumps formed at250°C for 1 h (Sample E).

However, in this study small size microbumps (25 and 10 µm) were composed of a single $(Cu,Co)_3Sn$ phase with no detectable voids. This could be an improvement in microbump reliability, as the main reasons for microbump failure are void formation and growth in microbumps during fabrication and operation. The current density in microbumps is much greater than that in joints of a larger size. Therefore, electromigration appears to be a major reliability issue for fine pitch interconnects (such as 25 and 10 µm microbumps). Electromigration accelerates void nucleation and growth. Hence, inhibiting the voids nucleation during the bonding can considerably enhance the microbumps' reliabiliy [8,75–77]. Furthermore, a joint composed of a single phase can show a higher reliability compared to a multi-phases joint. This is due to the fact that various diffusive characteristics of different phases causes a highly anisotropic conductivity and non-equilibrium concentration of vacancies in multi-phases joints. Hence, multi-phases joints are more likely prone to an electromigration failure than a single-phase joint [77–79].

3.2. Mechanical characterization

3.2.1. Tensile fracture surface

The tensile fracture surface of the 100nmCo/Sn-Cu joint (Sample B) was investigated. Fig. 7 shows a schematic of the tensile test setup and the BSE-SEM micrographs of the tensile fracture surface. According to the chemical analysis using EDX, Mo, $(Cu,Co)_6Sn_5$ with various amount of Co (2 at%, 5 at% and 8 at%), and $(Co,2at\%Cu)Sn_3$, and $(Cu,Co)_6Sn_5$ with various amount of Co (1 at%≤, 5 at% and 8 at%), and $(Co,2at\%Cu)Sn_3$ were identified at the Co-side and the Cu-side of the fracture surface, respectively. It should be noted that the $(Cu,5at\%Co)_6Sn_5$, $(Cu,8at\%Co)_6Sn_5$, and $(Co,Cu)Sn_3$ were also detected from a small fraction of the fracture surfaces. Therefore, these phases probably were too thin and did not grow along all the bond areas. Therefore, it was not possible to collect enough characteristic x-ray signals from $(Cu,8at\%Co)_6Sn_5$ and $(Co,Cu)Sn_3$ in the SEM-EDX analysis of the cross-sectional BSE-SEM image of sample B (Fig. 2-b).

Fig. 8 shows a schematic diagram of the fracture mode. The fracture path was as follows; inside the $(Cu,Co)_6Sn_5$ and $(Co,Cu)Sn_3$ phases, and at the Mo/IMCs interface. As can be seen in Fig. 7, the fracture surfaces were facet and irregular and rough. The

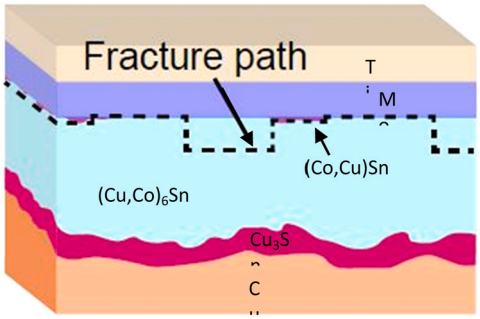

Fig. 8. Schematic diagram of the fracture mode of Sample B (Cu-Sn/Mo-100 nm Co).

simultaneous presence of facets and dimples shows the mixed ductile/brittle fracture mode. However, fully IMCs Cu-Sn joints mostly shows brittle fracture mode [80,81]. L. Sun et al. observed a relatively uniform and flat fracture surface for fully Cu-Sn IMCs joint and they described the fracture type as brittle [41]. According to L. Liu et al. both Cu_6Sn_5 and Cu_3Sn micro beams only shows elastic (linear) behaviour before failures [82]. However, the result in this study for Cu-Sn-Co SLID system revealed that the Co participation in the Cu-Sn IMCs formation probably decreases the brittleness of the Cu-Sn IMCs and correspondingly changes the brittle fracture mode of Cu-Sn SLID system to a mixed ductile/brittle fracture mode.

It is important to notice that the shear or tensile strength and the fracture mode significantly depend on the IMCs evolved in the bond area and their volume fraction [45]. Furthermore, it has been shown that the strengthening effect of the additive particles in Sn solder depends on the particle morphology. For instance, crack propagates along the Sn/IMC interface in the Sn bulk solders containing near-round shape Cu_6Sn_5 IMC. Nonetheless, a transgranular crack propagation observes in a Sn bulk solders containing $(Cu,Ni)_6Sn_5$ particles which show sunflower like morphology [83]. Hence, to study the morphologies of different IMCs identified in the fracture surface, the SEM-EDX in high-magnification was done in different part of the tensile fracture surfaces (Fig. 9). The results indicated that Cu_6Sn_5 with Co content less than 1 at% has almost the same morphology

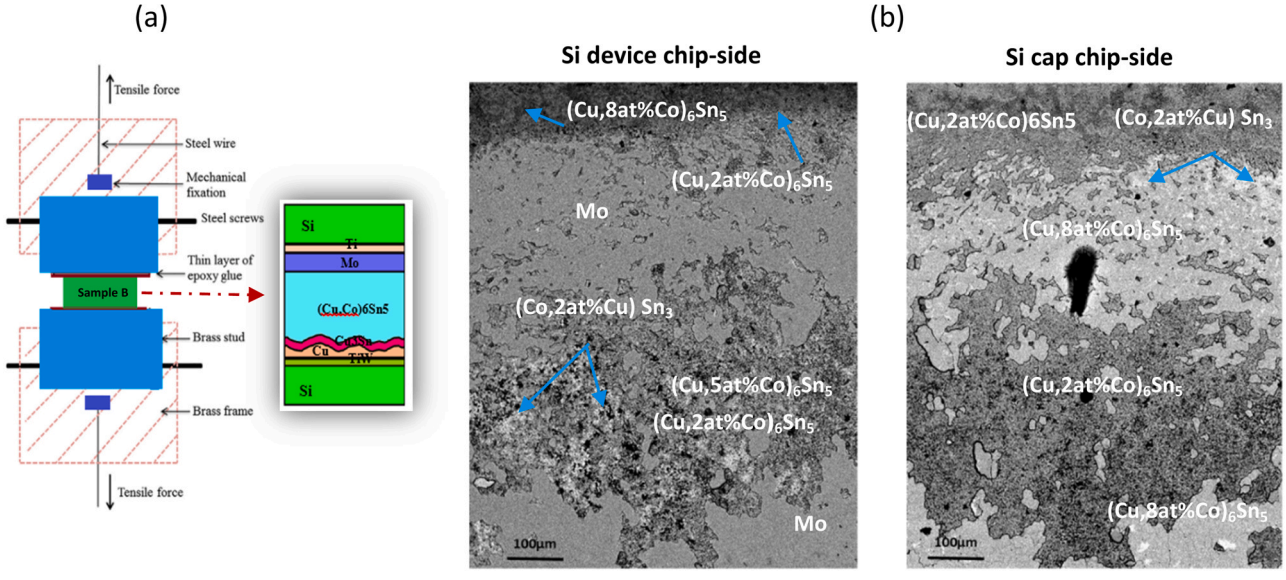

Fig. 7. (a) Schematic of tensile test setup, (b) BSE-SEM images of the tensile fracture surfaces of Sample B (Cu-Sn/Mo-100 nm Co).

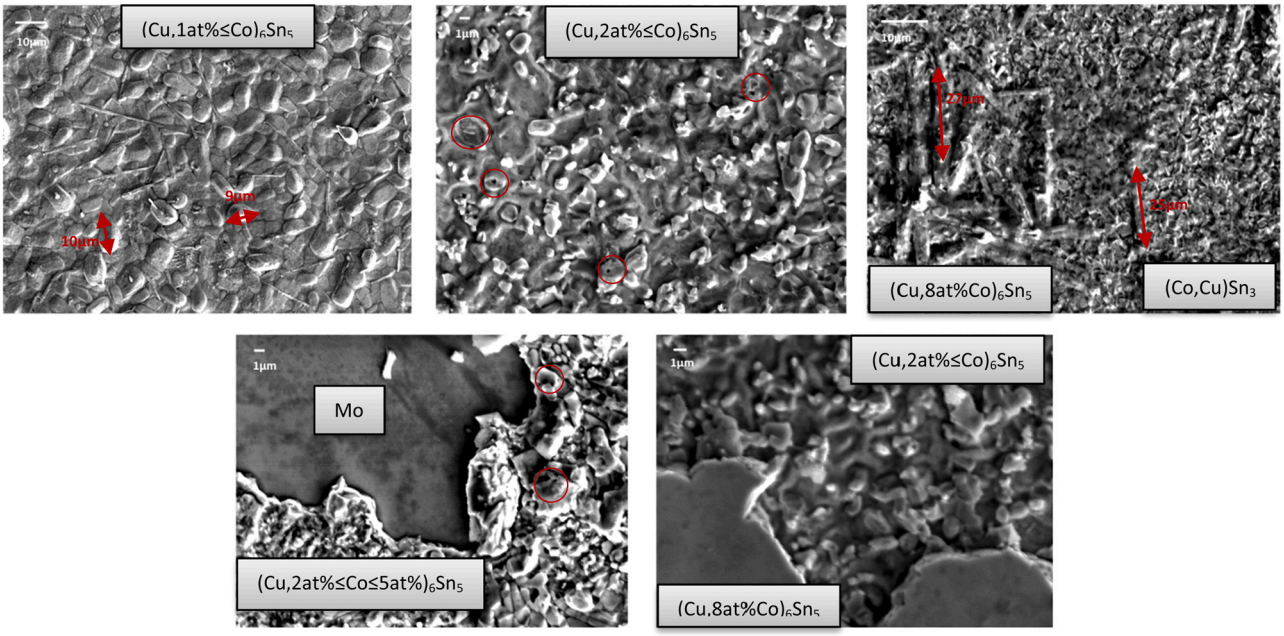

Fig. 9. The morphology of the IMCs identified in the tensile fracture surface.

(scalloped shape) as pure Cu_6Sn_5 reported in the literature (ref). The average grain size was measured to be about 8 µm. It seemed that the fracture propagated along the grain boundaries of the Cu_6Sn_5 with Co content ≤ 1 at%. However, higher Co content in the Cu_6Sn_5 drastically changed the Cu_6Sn_5 grain morphology from scalloped to dimple-like structure and finally to needle shape grains with average size of 25 µm for $(Cu,8at\%Co)_6Sn_5$. The $(Co,Cu)Sn_3$ phase with average size of 3 µm showed the same morphology (lath like) as $CoSn_3$ examined in the literature [81]. The $(Co,Cu)Sn_3$ IMCs exhibited an intergranular fracture which has been previously reported in the literature [81]. A portion of the fracture surface characterized by the Cu_6Sn_5 with 5 at%≥Co > 1 at% exhibited a dimple-like structure, which is an indication of ductile fracture mode. However, other parts of the fracture surface indicated the brittle fracture mode. Hence, it can be concluded that 100nmCo/Sn-Cu joint (Sample B) exhibited a mixed ductile-brittle fracture mode. This impact of Co on the reduction of the Cu-Sn IMCs' brittleness can be considered as an improvement for interconnection as the brittleness of IMCs were always a concern for fully IMCs joints [84–86].

3.2.2. Nano-indentation test

Fig. 10-a, -b, and -c show the cross-sectional BSE micrographs of Sample B (Mo-100 nm Co/Sn-Cu), Sample D (Mo-500 nm Co/Sn-Cu) and E (Cu/Sn/Cu) with marks of the nanoindentations, respectively. The nanoindentations were done at the joint area where $(Cu,Co)_6Sn_5$ phases were identified. After nanoindentation test, the EDX analysis was done to ensure that the indentation lied completely within $(Cu,Co)_6Sn_5$ IMC. The indentation load-displacement curves of $(Cu,Co)_6Sn_5$ and Cu_6Sn_5 are presented in Fig. 10-d. The nanoindentation hardness (H), reduced elastic modulus (Er), and Young's modulus (Ei) were calculated using Eqs. 1, 2, and 3 and the values are listed in Table 1. The measured Er and Ei for Cu_6Sn_5 in this study were below the average reported values in the literature (some reported values in the literature are listed in Table 1). However, it has to be considered that the mechanical properties of the Cu_3Sn and Cu_6Sn_5 strongly depend on the crystal orientation [7,12,14,65]. Besides, the strain rate can considerably affect the Young's modulus, elastic modulus and hardness values [93,94]. In the current study, the elastic modulus, Young's modulus, and hardness of Cu_6Sn_5 were found to increase as the Co content in the Cu_6Sn_5 IMC increases. It is worthwhile to note that the hardness value of the Cu_6Sn_5 IMC with low-Co content (on average 2 at%) is slightly larger than pure Cu_6Sn_5. However, the hardness value for the high-Co content (10 at%) Cu6Sn5 IMC is much larger than pure Cu_6Sn_5. Since E/H implies plasticity of the IMCs, higher E/H better plasticity and subsequently higher joint reliability, [7,95] it is important to consider the E/H values for IMCs formed in the joint area. The E/H values for Cu_6Sn_5, $(Cu,2at\%Co)_6Sn_5$, and $(Cu,10at\%Co)_6Sn_5$ were calculated to be 17, 20, and 17, respectively in this work. The E/H value for Cu_6Sn_5 in this study is in a good agreement with ref [95], and the E/H value for $(Cu,2at\%Co)_6Sn_5$ calculated in this study is much closer to the value for Cu_3Sn in ref [95]. According to the literature, a third element in Cu_6Sn_5 can affect young's modulus and hardness values [88,96,97]. However, the E/H values for Cu_6Sn_5 does not increase with previously studied third elements (such as Ni and Zn). For instance, E/H values for $(Cu,Ni)_6Sn_5$ with various amount of Ni is slightly below Cu_6Sn_5 [31,89,98,99]. Zn does not change the E/H value of Cu_6Sn_5 [97]. In the current study, we found that Co can change the E/H value of the Cu_6Sn_5 IMC. The results obtained from nanoindentation test regarding the plasticity (E/H values) are in a good agreement with the tensile fracture modes that were observed in this study. The fracture surface analyses indicated that Co-Sn-Cu SLID system shows mixed ductile-brittle fracture mode. The dimple morphology of Cu_6Sn_5 with 5 at%≥Co content > 1 at% is an indication of ductile fracture mode. Therefore, it can be concluded that Cu_6Sn_5 with 5 at %≥Co content > 1 at% has some order of plasticity which was confirmed with a larger E/H value for Cu_6Sn_5 with 2 at% Co on average compared to pure Cu_6Sn_5.

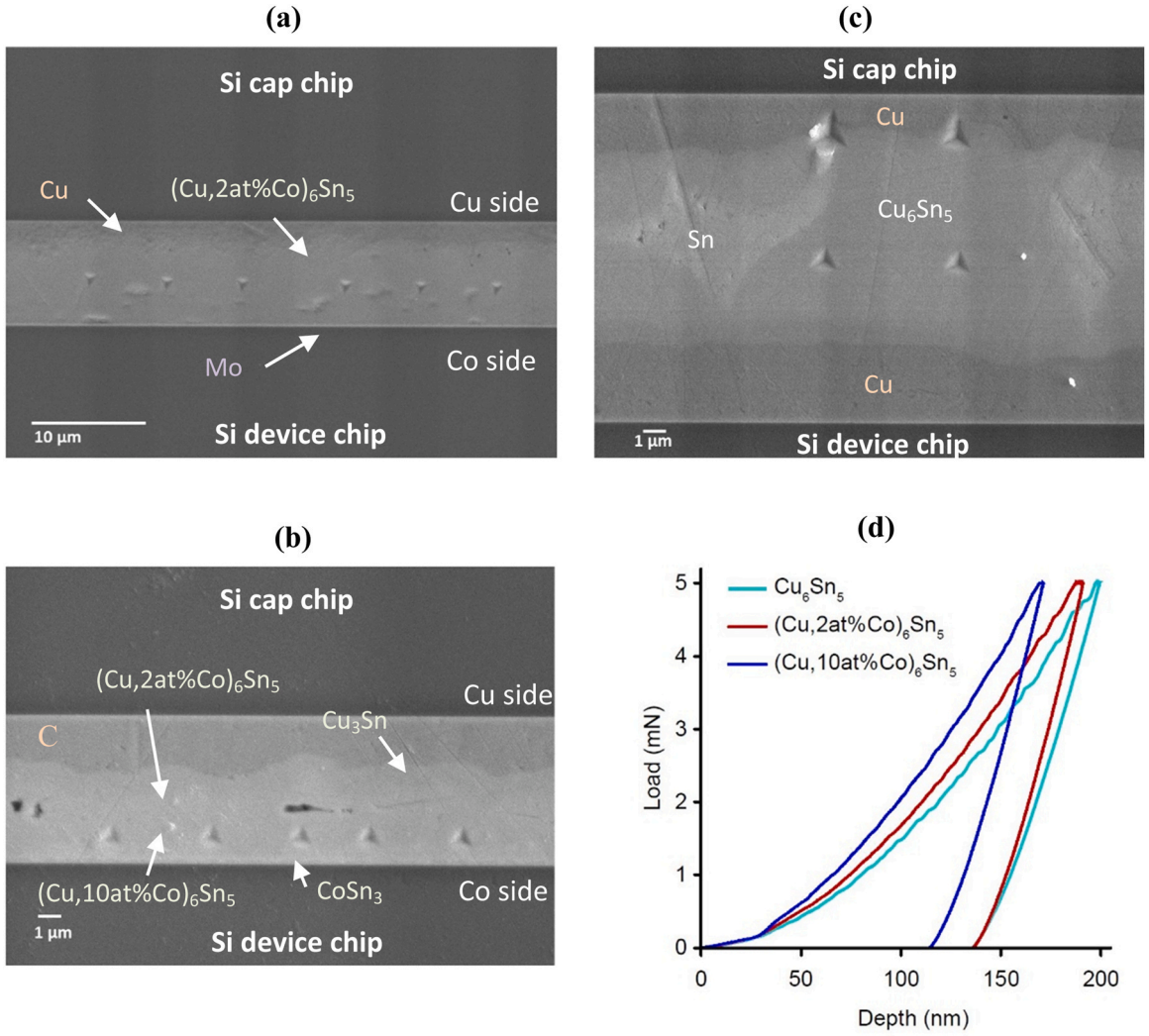

Fig. 10. BSE SEM image of indents on (a) Sample B (Cu-Sn/Mo-100 nm Co) bonded at 250 C for 1 h, (b) Sample D (Cu-Sn/Mo-500 nm Co) bonded at 250 C for 1 h, and (C) Sample E (Cu/Sn/Cu) bonded at 250 C for 20 min, and (d) the indentation load displacement curves of Cu6Sn5, (Cu,2at%Co)6Sn5, and (Cu,10at%Co)6Sn5 IMCs.

Table 1
The nanoindentation hardness (H), reduced elastic modulus (Er), and Young's modulus (Ei) of Cu6Sn5 with various Co content obtained from this study and the literature.

	$(Cu,2at\%Co)_6Sn_5$	$(Cu,10at\%Co)_6Sn_5$	Cu_6Sn_5	Reported value of Cu_6Sn_5
Elastic Modulus(Gpa)	122 ± 6	134 ± 5	103 ± 1	125 ± 7[87], 106 ± 3[88], 111 ± 3[6], 101 ± 3[89],
Young's Modulus(Gpa)	136 ± 8	151 ± 7	114 ± 1	125 ± 7[90], 120 ± 4[91], 97 ± 3[92]
Hardness(Gpa)	6.9 ± 0.2	8.9 ± 0.2	6.7 ± 0.4	6.7 ± 0.4[87], 6.1 ± 0.5[90], 5.6 ± 0.3[91], 5.7 ± 0.2[88], 6.6 ± 0.4[6], 5.8 ± 0.4[89], 5.7 ± 0.5[92]

4. Conclusion

To conclude, this work elaborates on both the optimization of a physically deposited contact metallization stack for Cu-Sn SLID systems and the mechanical characterization of the joint (Co-Sn-Cu SLID system). Four different contact metallization stacks for (4 µm Cu-2 µm Sn) SLID system were investigated: A) Ti-100 nm Co, B) Ti-Mo-100 nm Co, C) Ti-500 nm Co, and D) Ti-Mo-500 nm Co. Depending on the contact metallization stack layers, reaction products were (Cu,Co)6Sn5 with various Co contents, (Co,Cu)Sn3, and Cu3Sn. The SEM cross-sectional study of the joints demonstrated that the Ti/IMCs interface exhibits a low reliability and can be a place of the joint detachment. Consequently, it is crucial to apply an intermediate layer such as Mo (between Ti and Co) in the metallization stack in order to increase the joint reliability. Furthermore, the formation of the (Cu,Co)6Sn5 IMC with high Co content deteriorated the bond quality, which was widely discussed in our previous work [46] and confirmed in the current work. Hence, it is essential to consider the limitation of the tCo / tSn ratio to inhibit the formation of the Cu6Sn5 with high Co content. In sample B (Mo-100 nm Co/Cu-Sn), both considerations; tCo/tSn ratio limitation and utilizing a Mo interlayer between Ti and Co- were applied for the contact metallization stack design. The joint contained the Cu3Sn and (Cu, Co) 6Sn5 IMCs with high-quality (void- and crack-free). The thermal aging study revealed that the void formation can be significantly reduced with the presence of Co in the Cu6Sn5 phase. In addition, the mechanical properties of the joint improved compared to Cu-Sn-Cu SLID system: 1) both facets and dimples were observed in the tensile fracture surface of the joint, indicating mixed ductile/brittle fracture mode; 2) the (Cu,2at%Co)6Sn5 IMC in the Co-Sn-Cu system showed higher Young's modulus and E/H values than Cu6Sn5 formed in Cu-Sn system. Hence, the plasticity of 4 µm Cu-2 µm Sn

SLID system improves by utilizing Ti/Mo/100 nm Co contact metallization stack. Furthermore, this study showed that void free small microbumps (down to 10 µm) can be achieved by utilizing Ti-Mo-100 nm Co contact metallization stack for 2 µm Sn-4 µm Cu SLID system.

The proposed contact metallization stack (Ti-Mo-Co with the tCo/tSn = 0.05) for Cu-Sn SLID systems benefits the microsystem, microelectromechanical systems, and microelectronics packaging in two ways: 1) Process simplification through avoiding chemical processes including Cu electroplating on the device wafers (such as fragile MEMS devices), and 2) Reliability improvement due to the higher joint's plasticity and a smaller number of voids in the bonding area even after long-time annealing. For instance, a smaller number of voids in a joint can be highly profitable for small size microbumps packaging, as the main reason for their failure is void formation and growth in microbumps joint during fabrication and operation.

Funding

The authors would like to acknowledge the Innovation Funding Agency Business Finland for their financial support. The work has been carried out as part of "Silicon microfabrication platform development for next generation products - Beyond SOI" project (1364/31/2019).

CRediT authorship contribution statement

M. Paulasto-Kröckel: Supervision, Conceptualization, Writing – review & editing. **V. Vuorinen:** Project administration, Conceptualization, Writing – review & editing. **S. Mertin:** Sputtering of thin film metallization stack. **K. Widell:** Operating nano-indenter tool. **F. Emadi:** Formal analysis, Investigation, Writing – original draft, Visualization.

Data Availability

Data will be made available on request.

Declaration of Competing Interest

The authors declare that they have no known competing financial interests or personal relationships that could have appeared to influence the work reported in this paper.

Acknowledgment

We acknowledge the provision of facilities and technical support by Aalto University at OtaNano-Nanomicroscopy Center (Aalto- NMC).

References

[1] N. Hoivik et al., Fluxless wafer-level Cu-Sn bonding for micro- and nanosystems packaging, Electron. Syst. Integr. Technol. Conf. ESTC 2010 - Proc., 2010.
[2] H.K. Kannojia, S.K. Sharma, P. Dixit, Void formation and intermetallic growth in pulse electrodeposited Cu-Sn layers for MEMS packaging, J. Electron. Mater. 47 (12) (2018) 7386–7400.
[3] Z. Wu, J. Cai, Q. Wang, J. Wang, D. Wang, Wafer-level hermetic package by low-temperature Cu/Sn TLP bonding with optimized Sn thickness, J. Electron. Mater. 46 (10) (2017) 6111–6118.
[4] O. Temel, Y.E. Kalay, T. Akin, Wafer-level low-temperature solid-liquid inter-diffusion bonding with thin Au-Sn layers for MEMS encapsulation, J. Micro Syst. 30 (1) (2021) 64–71.
[5] L. Skogström, J. Li, T.T. Mattila, V. Vuorinen, "MEMS reliability," in Handbook of Silicon Based MEMS Materials and Technologies, 2020, pp. 851–876.
[6] D. Mu, H. Yasuda, H. Huang, K. Nogita, Growth orientations and mechanical properties of Cu6Sn5 and (Cu,Ni)6Sn5 on poly-crystalline Cu (Sep.), J. Alloy. Compd. 536 (2012) 38–46 (Sep.).
[7] J.-M. Song, B.-C. Hung, D. Tarng, C.-P. Hung, K. Yasuda, Relationship between nanomechanical response of interfacial intermetallic compound layers and impact reliability of solder joints, Nanomaterials 10 (1456) (2020) 539–547.
[8] M.S. Park, S.L. Gibbons, R. Arróyave, Phase-field simulations of intermetallic compound growth in Cu/Sn/Cu sandwich structure under transient liquid phase bonding conditions, Acta Mater. 60 (18) (2012) 6278–6287.
[9] T.L. Yang, et al., Full intermetallic joints for chip stacking by using thermal gradient bonding, Acta Mater. 113 (2016) 90–97.
[10] B.S. Lee, J.W. Yoon, Cu-Sn intermetallic compound joints for high-temperature power electronics applications, J. Electron. Mater. 47 (1) (2018) 430–435.
[11] T.T. Luu, A. Duan, K. Wang, K.E. Aasmundtveit, N. Hoivik, "Optimization of Cu/Sn wafer-level bonding based upon intermetallic characterization," 2012 4th Electron. Syst. Technol. Conf. ESTC 2012, 2012.
[12] Z. Li, M. Li, Y. Xiao, C. Wang, Ultrarapid formation of homogeneous Cu6Sn5 and Cu3Sn intermetallic compound joints at room temperature using ultrasonic waves (May), Ultrason. Sonochem. 21 (3) (2014) 924–929 (May).
[13] T.T. Luu, A. Duan, K. Wang, K. Aasmundtveit, N. Hoivik, Cu/Sn SLID wafer-level bonding optimization, Proc. - Electron. Components Technol. Conf., pp. 1531–1537, 2013.
[14] M. Li, Z. Li, Y. Xiao, C. Wang, Rapid formation of Cu/Cu3Sn/Cu joints using ultrasonic bonding process at ambient temperature (Mar.), Appl. Phys. Lett. 102 (9) (2013) 094104(Mar.).
[15] L. Xu, J.H.L. Pang, Nano-indentation characterization of Ni-Cu-Sn IMC layer subject to isothermal aging, Thin Solid Films 504 (1–2) (2006) 362–366.
[16] J.Y. Wu, Y.S. Chiu, Y.W. Wang, C.R. Kao, Mechanical characterizations of single-crystalline (Cu, Ni) 6 Sn 5 through uniaxial micro-compression (no. March), Mater. Sci. Eng. A 753 (2019) 22–30.
[17] G. Ross, P. Malmberg, V. Vuorinen, M. Paulasto-Kröckel, The role of ultrafine crystalline behavior and trace impurities in copper on intermetallic void formation, ACS Appl. Electron. Mater. 1 (1) (2019) 88–95.
[18] G. Ross, V. Vuorinen, M. Paulasto-Kröckel, Void formation and its impact on Cu-Sn intermetallic compound formation, J. Alloy. Compd. 677 (2016) 127–138.
[19] J.Y. Kim, J. Yu, S.H. Kim, Effects of sulfide-forming element additions on the Kirkendall void formation and drop impact reliability of Cu / Sn – 3. 5Ag solder joints, Acta Mater. 57 (17) (2009) 5001–5012.
[20] J. Yu, J.Y. Kim, Effects of residual S on Kirkendall void formation at Cu / Sn – 3. 5Ag solder joints, Acta Mater. 56 (19) (2008) 5512–5521.
[21] H.K. Kannojia, P. Dixit, A review of intermetallic compound growth and void formation in electrodeposited Cu–Sn Layers for microsystems packaging, J. Mater. Sci. Mater. Electron. 32 (6) (2021) 6742–6777.
[22] P.-C. Chiang, Y.-A. Shen, S.-P. Feng, C.-M. Chen, Electrodeposition of twinned Cu with strong texture effect on voiding propensity in electroplated Cu solder joints, J. Electrochem. Soc. 167 (16) (2020) 162516.
[23] F. Somidin, et al., Direct observation of the Ni stabilising effect in interfacial (Cu,Ni)6Sn5 intermetallic compounds, no. October 2019, Materialia 9 (2020) 100530.
[24] T. Laurila, J. Hurtig, V. Vuorinen, J.K. Kivilahti, Effect of Ag, Fe, Au and Ni on the growth kinetics of Sn-Cu intermetallic compound layers, Microelectron. Reliab. 49 (3) (2009) 242–247.
[25] G. Zeng, et al., Phase stability and thermal expansion behavior of Cu6Sn 5 intermetallics doped with Zn, Au and in, Intermetallics 43 (2013) 85–98.
[26] H.K. Kannojia, P. Dixit, A review of intermetallic compound growth and void formation in electrodeposited Cu–Sn Layers for microsystems packaging, J. Mater. Sci.: Mater. Electron. 32 (6) (2021) 6742–6777.
[27] C.Y. Yu, J.G. Duh, Stabilization of hexagonal Cu6(Sn,Zn)5 by minor Zn doping of Sn-based solder joints, Scr. Mater. 65 (9) (2011) 783–786.
[28] K. Nogita, M.A.A.M. Salleh, E. Tanaka, G. Zeng, S.D. Mcdonald, S. Matsumura, "In Situ TEM Observations of Cu 6 Sn 5 Polymorphic Transformations in Reaction Layers Between Sn-0.7Cu Solders and Cu Substrates," vol. 68.
[29] K. Nogita, T. Nishimura, Nickel-stabilized hexagonal (Cu, Ni)6Sn5 in Sn-Cu-Ni lead-free solder alloys, Scr. Mater. 59 (2) (2008) 191–194.
[30] A. Rautiainen, G. Ross, V. Vuorinen, H. Dong, M. Paulasto-Kröckel, The effect of platinum contact metallization on Cu/Sn bonding, J. Mater. Sci. Mater. Electron. 29 (17) (2018) 15212–15222.
[31] D. Mu, H. Huang, S.D. McDonald, J. Read, K. Nogita, Investigating the mechanical properties, creep and crack pattern of Cu6Sn5 and (Cu,Ni)6Sn5 on diverse crystal planes, Mater. Sci. Eng. A 566 (2013) 126–133.
[32] Z. Yin, F. Sun, M. Guo, Investigation of elevated temperature mechanical properties of intermetallic compounds in the Cu-Sn system using nanoindentation, J. Electron. Packag. Trans. ASME 142 (2) (2020) 1–7.
[33] J. Feng, C. Hang, Y. Tian, C. Wang, B. Liu, Effect of electric current on grain orientation and mechanical properties of Cu-Sn intermetallic compounds joints, J. Alloy. Compd. 753 (2018) 203–211.
[34] Y.V. Milman, B.A. Galanov, S.I. Chugunova, Plasticity characteristic obtained through hardness measurement, Acta Met. Mater. 41 (9) (1993) 2523–2532.
[35] J.M. Song, B.R. Huang, C.Y. Liu, Y.S. Lai, Y.T. Chiu, T.W. Huang, Nanomechanical responses of intermetallic phase at the solder joint interface - Crystal orientation and metallurgical effects, Mater. Sci. Eng. A v534, (2012) 53–59.
[36] J.M. Song, Y.L. Shen, C.W. Su, Y.S. Lai, Y.T. Chiu, Strain rate dependence on nanoindentation responses of interfacial intermetallic compounds in electronic solder joints with Cu and Ag substrates, Mater. Trans. 50 (5) (2009) 1231–1234.
[37] "Rapid fabrication of Cu_40-µm thick full Cu3Sn_Cu joints by applying pulsed high frequency electromagnetic field for high power electronics _ Elsevier Enhanced Reader.pdf.".

[38] X. Han, X. Li, P. Yao, D. Chen, Influence of ultrasounds on interfacial microstructures of Cu-Sn solder joints, Solder. Surf. Mt. Technol. 33 (4) (2020) 206–214.

[39] "A comparative study of Cn_Sn_Cu and Ni_Sn_Ni solder joints for low temperature stable transient liquid phase bonding _ Elsevier Enhanced Reader.pdf.".

[40] M.A. Bassi, M.A. Lopez, L. Confalone, R.M. Gaudio, L. Lombardo, D. Lauritano, Enhanced Reader.pdf, Nature 388 (2020) 539–547.

[41] L. Sun, M. he Chen, L. Zhang, Microstructure evolution and grain orientation of IMC in Cu-Sn TLP bonding solder joints, J. Alloy. Compd. 786 (2019) 677–687.

[42] H. Tatsumi, et al., Evolution of transient liquid-phase sintered Cu-Sn skeleton microstructure during thermal aging, Appl. Sci. 9 (1) (2019).

[43] B.S. Lee, J.W. Yoon, Cu-Sn intermetallic compound joints for high-temperature power electronics applications, J. Electron. Mater. 47 (1) (2018) 430–435.

[44] "Microstructure, interfacial reactions and mechanical properties of Co_Sn_Co and Cu_Sn_Cu joints produced by transient liquid phase bonding _ Enhanced Reader.pdf.".

[45] P. Yao, X. Li, X. Han, L. Xu, Shear strength and fracture mechanism for full Cu-Sn IMCs solder joints with different Cu3Sn proportion and joints with conventional interfacial structure in electronic packaging, Solder. Surf. Mt. Technol. 31 (1) (2019) 6–19.

[46] F. Emadi, V. Vuorinen, H. Dong, G. Ross, M. Paulasto-Kröckel, Investigation of the microstructural evolution and detachment of Co in contact with Cu–Sn electroplated silicon chips during solid-liquid interdiffusion bonding, J. Alloy. Compd. 890 (2022) 161852.

[47] J.H. Liu, et al., Study on the microstructure and mechanical properties of Cu-Sn intermetallic joints rapidly formed by ultrasonic-assisted transient liquid phase soldering, J. Alloy. Compd. 692 (2017) 552–557.

[48] Z. Yin, F. Sun, M. Guo, The fast formation of Cu-Sn intermetallic compound in Cu/Sn/Cu system by induction heating process, Mater. Lett. 215 (2018) 207–210.

[49] H.J. Dong, et al., Grain morphology evolution and mechanical strength change of intermetallic joints formed in Ni/Sn/Cu system with variety of transient liquid phase soldering temperatures (no. August), Mater. Sci. Eng. A 705 (2017) 360–365.

[50] Q. Guo, S. Sun, Z. Zhang, H. Chen, M. Li, Microstructure evolution and mechanical strength evaluation in Ag/Sn/Cu TLP bonding interconnection during aging test, no. August 2017, Microelectron. Reliab. 80 (2018) 144–148.

[51] L. Mo, C. Guo, Z. Zhou, F. Wu, C. Liu, Microstructural evolution of Cu–Sn–Ni compounds in full intermetallic micro-joint and in situ micro-bending test, J. Mater. Sci. Mater. Electron. 29 (14) (2018) 11920–11929.

[52] L. Mo, Z. Zhou, F. Wu, S. Liu, H. Liu, and C. Liu, Mechanical property of Cu-Sn-Ni intermetallics in the full intermetallic micro-joints formed with transient liquid phase soldering, 18th Int. Conf. Electron. Packag. Technol. ICEPT 2017, pp. 1046–1050, 2017.

[53] Z.L. Li, et al., Homogeneous (Cu, Ni)6Sn5 intermetallic compound joints rapidly formed in asymmetrical Ni/Sn/Cu system using ultrasound-induced transient liquid phase soldering process, no. October 2017, Ultrason. Sonochem. 42 (2018) 403–410.

[54] A. Rautiainen, V. Vuorinen, H. Heikkinen, M. Paulasto-Krockel, Wafer-level AuSn/Pt solid-liquid interdiffusion bonding, IEEE Trans. Compon. Packag. Manuf. Technol. vol. 8, (2) (2018) 169–176.

[55] Y.L. Tseng, Y.C. Chang, C.C. Chen, Co Effects upon Intermetallics Growth Kinetics in Sn-Cu-Co/Ni and Sn-Cu-Co/Cu Couples, J. Electron. Mater. 44 (1) (2015) 581–589.

[56] J. Fan, et al., Effect of Co content on the microstructure, spreadability, conductivity and corrosion resistance of Sn-0.7Cu alloy (no. February), Microelectron. Reliab. 107 (2020) 113615.

[57] C.H. Wang, C.C. Wen, C.Y. Lin, Solid-state interfacial reactions of Sn and Sn-Ag-Cu solders with an electroless Co(P) layer deposited on a Cu substrate, J. Alloy. Compd. 662 (2016) 475–483.

[58] H. Gao, F. Wei, Y. Sui, J. Qi, Growth behaviors of intermetallic compounds on the Sn-0.7Cu-10Bi-xCo/Co interface during multiple reflow, Mater. Des. 174 (2019) 107794.

[59] C. Du, X. Wang, S. Tian, Effect of bonding time on the microstructure and mechanical properties of Co / Sn / Cu joint, J. Mater. Sci. Mater. Electron. 29 (2018) 455–466.

[60] C.H. Wang, C.Y. Kuo, Growth kinetics of the solid-state interfacial reactions in the Sn-Cu/Co and Sn/Co-Cu couples, Mater. Chem. Phys. 130 (1–2) (2011) 651–656.

[61] C. chi Chen, Y. lun Tseng, Cross-interaction in Cu/Sn/Co/Sn/Ni and Cu/Sn–Co/Co/Sn– Co/Ni couples, J. Electron. Mater. 44 (3) (2015) 1021–1027.

[62] K.C. Huang, et al., Study of interfacial reactions between Sn(Cu) solders and Ni-Co alloy Layers, J. Electron. Mater. 39 (11) (2010) 2403–2411.

[63] H.P. Park, G. Seo, S. Kim, K. one Ahn, Y.H. Kim, Shear strength between Sn–3.0Ag–0.5Cu solders and Cu substrate after two solid-state aging processes for fan-out package process applications, J. Mater. Sci. Mater. Electron. 30 (11) (2019) 10550–10559.

[64] H.P. Park, G. Seo, S. Kim, K. one Ahn, Y.H. Kim, Shear strength between Sn–3.0Ag–0.5Cu solders and Cu substrate after two solid-state aging processes for fan-out package process applications, J. Mater. Sci. Mater. Electron. 30 (11) (2019) 10550–10559.

[65] P.G. Kim, J.W. Jang, T.Y. Lee, K.N. Tu, Interfacial reaction and wetting behavior in eutectic SnPb solder on Ni/Ti thin films and Ni foils, J. Appl. Phys. 86 (12) (1999) 6746–6751.

[66] "Dewetting of molten Sn on Au_Cu_Cr thin-film metallization _ Enhanced Reader.pdf.".

[67] C.H. Tsai, S.Y. Lin, P.T. Lee, C.R. Kao, A new spalling mechanism of intermetallics from the adhesion layer in the terminal-stage reaction between Cu and Sn, Intermetallics 138 (2021).

[68] A.A. Liu, H.K. Kim, K.N. Tu, P.A. Totta, Spalling of Cu6Sn5 spheroids in the soldering reaction of eutectic SnPb on Cr/Cu/Au thin films, J. Appl. Phys. 80 (5) (1996) 2774–2780.

[69] G.Z. Pan, A.A. Liu, H.K. Kim, K.N. Tu, P.A. Totta, Microstructures of phased-in Cr-Cu/Cu/Au bump-limiting metallization and its soldering behavior with high Pb content and eutectic PbSn solders, Appl. Phys. Lett. 71 (20) (1997) 2946–2948.

[70] F. Gao, T. Takemoto, H. Nishikawa, Effects of Co and Ni addition on reactive diffusion between Sn-3.5Ag solder and Cu during soldering and annealing, Mater. Sci. Eng. A 420 (1–2) (2006) 39–46.

[71] Y.W. Wang, Y.W. Lin, C.T. Tu, C.R. Kao, Effects of minor Fe, Co, and Ni additions on the reaction between SnAgCu solder and Cu, J. Alloy. Compd. 478 (1–2) (2009) 121–127.

[72] G. Ross, "Intermetallic Void Formation in Cu-Sn Micro-Connects," 2019.

[73] S. Bordère, E. Feuillet, J.L. Diot, R. de Langlade, J.F. Silvain, Understanding of void formation in Cu/Sn-Sn/Cu system during transient liquid phase bonding process through diffusion modeling, Metall. Mater. Trans. B Process. Metall. Mater. Process. Sci. 49 (6) (2018) 3343–3356.

[74] Q. Li, Y.C. Chan, Growth kinetics of the Cu3Sn phase and void formation of submicrometre solder layers in Sn – Cu binary and Cu – Sn – Cu sandwich structures, J. Alloy. Compd. 567 (2013) 47–53.

[75] M.B. Kelly, S. Niverty, N. Chawla, Four dimensional (4D) microstructural evolution of Cu6Sn5 intermetallic and voids under electromigration in bi-crystal pure Sn solder joints (May), Acta Mater. 189 (2020) 118–128 (May).

[76] Y.W. Chang, et al., Study of electromigration-induced formation of discrete voids in flip-chip solder joints by in-situ 3D laminography observation and finite-element modeling (Sep.), Acta Mater. 117 (2016) 100–110 (Sep.).

[77] V. Attari, S. Ghosh, T. Duong, R. Arroyave, On the interfacial phase growth and vacancy evolution during accelerated electromigration in Cu/Sn/Cu microjoints (Nov.), Acta Mater. 160 (2018) 185–198 (Nov.).

[78] Y. chen Liu, Y. si Yu, S. kang Lin, S.J. Chiu, Electromigration effect upon single- and two-phase Ag-Cu alloy strips: An in situ study (Dec.), Scr. Mater. 173 (2019) 134–138 (Dec.).

[79] Z.J. Morgan, Y.M. Jin, Phase field modeling of pore electromigration in anisotropic conducting polycrystals (Feb.), Comput. Mater. Sci. 172 (2020) 109362(Feb.).

[80] L. Sun, M. he Chen, L. Zhang, Microstructure evolution and grain orientation of IMC in Cu-Sn TLP bonding solder joints (May), J. Alloy. Compd. 786 (2019) 677–687 (May).

[81] S. Tian, J. Zhou, F. Xue, R. Cao, F. Wang, Microstructure, interfacial reactions and mechanical properties of Co/Sn/Co and Cu/Sn/Cu joints produced by transient liquid phase bonding, J. Mater. Sci. Mater. Electron. 29 (19) (2018) 16388–16400.

[82] L. Liu, Z. Chen, C. Liu, Y. Wu, B. An, Micro-mechanical and fracture characteristics of Cu6Sn5 and Cu3Sn intermetallic compounds under micro-cantilever bending, Intermetallics 76 (2016) 10–17.

[83] B. Wang, F. Wu, Y. Wu, B. An, H. Liu, J. Zou, A comparative study of microstructure and mechanical properties among Cu/Sn/Cu, Ni/Sn/Ni and Cu/Sn/Ni solder joints, Solder. Surf. Mt. Technol. 23 (1) (2011) 40–46.

[84] J. Hektor, M. Ristinmaa, H. Hallberg, S.A. Hall, S. Iyengar, Coupled diffusion-deformation multiphase field model for elastoplastic materials applied to the growth of Cu6Sn5 (Apr.), Acta Mater. 108 (2016) 98–109 (Apr.).

[85] A. Durga, P. Wollants, N. Moelans, Phase-field study of IMC growth in Sn–Cu/Cu solder joints including elastoplastic effects (Apr.), Acta Mater. 188 (2020) 241–258 (Apr.).

[86] W. Yue, Z. Zhang, B. Liang, J. Li, C. Xue, "Inner microcrack induced by intermetallic compound in right-angle Au/Sn3.0Ag0.5Cu/Au solder joints," 2021 22nd Int. Conf. Electron. Packag. Technol. ICEPT 2021, Sep. 2021.

[87] Z. Yin, F. Sun, M. Guo, Investigation of elevated temperature mechanical properties of intermetallic compounds in the Cu-Sn system using nanoindentation (Jun.), J. Electron. Packag. Trans. ASME 142 (2) (2020) (Jun.).

[88] D. Mu, H. Huang, S.D. McDonald, J. Read, K. Nogita, Investigating the mechanical properties, creep and crack pattern of Cu6Sn5 and (Cu,Ni)6Sn5 on diverse crystal planes (Mar.), Mater. Sci. Eng. A 566 (2013) 126–133 (Mar.).

[89] A. Fahim, S. Ahmed, J.C. Suhling, and P. Lall, Mechanical Characterization of Intermetallic Compounds in SAC Solder Joints at Elevated Temperatures, Proc. 17th Intersoc. Conf. Therm. Thermomechanical Phenom. Electron. Syst. ITherm 2018, pp. 1081–1090, Jul. 2018.

[90] G.Y. Jang, J.W. Lee, J.G. Duh, The nanoindentation characteristics of Cu6Sn5, Cu3Sn, and Ni3Sn4 intermetallic compounds in the solder bump, J. Electron. Mater. 2004 3310 33 (10) (2004) 1103–1110.

[91] J. Feng, C. Hang, Y. Tian, C. Wang, B. Liu, Effect of electric current on grain orientation and mechanical properties of Cu-Sn intermetallic compounds joints (Jul.), J. Alloy. Compd. 753 (2018) 203–211 (Jul.).

[92] F.X. Che, J.H.L. Pang, Characterization of IMC layer and its effect on thermo-mechanical fatigue life of Sn-3.8Ag-0.7Cu solder joints, J. Alloy. Compd. 541 (2012) 6–13.

[93] H. Jun, et al., Anomalous multiple pop-in behavior in Cu-Sn-based intermetallic compounds during nanoindentation, Mater. Sci. Eng. A 612 (2014) 192–196.

[94] J.M. Song, W.C. Lu, P.W. Chou, Nanomechanical responses of an intermetallic compound layer in transient liquid phase bonding using indium, J. Electron. Mater. 49 (1) (2020) 18–25.

[95] J.M. Song, Y.R. Liu, Y.S. Lai, Y.T. Chiu, N.C. Lee, Influence of trace alloying elements on the ball impact test reliability of SnAgCu solder joints, Microelectron. Reliab. 52 (1) (2012) 180–189.
[96] D. Mu, H. Huang, K. Nogita, Anisotropic mechanical properties of Cu 6Sn 5 and (Cu,Ni) 6Sn 5, Mater. Lett. 86 (2012) 46–49.
[97] C.Y. Yu, W.Y. Chen, J.G. Duh, Improving the impact toughness of Sn-Ag-Cu/Cu-Zn Pb-free solder joints under high speed shear testing, J. Alloy. Compd. 586 (2014) 633–638.
[98] D. Mu, H. Huang, S.D. McDonald, K. Nogita, Creep and mechanical properties of Cu6Sn5 and (Cu,Ni)6Sn5 at elevated temperatures, J. Electron. Mater. 42 (2) (2013) 304–311.
[99] D. Mu, H. Yasuda, H. Huang, K. Nogita, Growth orientations and mechanical properties of Cu 6Sn 5 and (Cu,Ni) 6Sn 5 on poly-crystalline Cu, J. Alloy. Compd. 536 (2012) 38–46.